Analytical Critical Phenomena of Rotating Regular AdS Black Holes with Dark Energy

H. Laassiri^{1*}, A. Daassou^{1†}, R. Benbrik^{1‡}

¹Fundamental and Applied Physics Laboratory, Physics Department, Polydisciplinary Faculty, Cadi Ayyad University, Sidi Bouzid, B.P. 4162, Safi, Morocco.

Abstract

This study focuses on precisely calculating analytical critical points for rotating regular AdS black holes, examining scenarios with and without external dark field contributions. Importantly, it represents the first attempt to compute critical points for this specific class of rotating black holes. Our primary focus is on investigating the impact resulting from variations in the charge of nonlinear electrodynamics on the critical phenomena of rotating regular AdS black holes, while also incorporating the influence of quintessence field contributions. The analytical investigation is concentrated on the horizon radius, employing two distinct approaches to simplify the complexity and length of the calculations. Furthermore, our examination extends to deciphering the intricate relationship between dark energy and critical phenomena. This involves visually portraying a range of critical behaviors and detailing a recent discovery regarding how the intensity of quintessence affects phase transitions. The shift in these transitions conform to either a concave or convex function, a characteristic dependent on the sign of quintessence intensity.

Keywords: Dark energy; Critical phenomena; Rotating regular AdS black holes; Phase transition.

^{*}hayat.laassiri@gmail.com

[†]ahmed.daassou@uca.ma

[‡]r.benbrik@uca.ac.ma

1 Introduction

The existence of singularities signifies the inability to predict specific physical phenomena, underscoring the inadequacy of general relativity. Fortunately, attempts have been undertaken to overcome singularities, including the incorporation of regular black holes. Bardeen's creation of a regular black hole [1] demonstrates this approach, incorporating ideas from the theory of quantum gravity and substituting central singularities with matter backgrounds. As the Bardeen solution did not satisfy the vacuum Einstein equations, Beato and Garcia demonstrated that by considering the coupling of gravitational theory with nonlinear electrodynamics, one could derive this solution [2]. The exploration of regular solutions has been extensively pursued in the literature, showcasing a multitude of proposed solutions and comprehensive analyses of their properties [3–7]. This reflects a substantial body of work dedicated to understanding and expanding upon the implications of incorporating nonlinear electrodynamics in gravitational theory.

There are similar aspects between non-linear electrodynamics and Hayward-Bardeen black holes. To begin, both involve non-linear effects. In electrodynamics, this is evident in the form of non-linear equations describing the electromagnetic field, while in the context of Hayward-Bardeen black holes, non-linearity arises from modifications to the Einstein field equations due to the presence of exotic matter or scalar fields [8,9] Moreover, both non-linear electrodynamics and Hayward-Bardeen black holes influence the interaction between gravitational and electromagnetic fields. Non-linear electrodynamics introduces corrections to the electromagnetic field equations, potentially affecting the behavior of charged particles in curved spacetime. Similarly, Hayward-Bardeen black holes modify the gravitational field around them, consequently impacting the behavior of electromagnetic fields in their vicinity [10].

Extensive discussions in [11–17] focused on how the quintessential parameter impacts the quasinormal frequencies across various black hole spacetimes. In reference to [18], the authors investigated the Bardeen solution, incorporating a cosmological constant and surrounded it by quintessence. Their study revealed that this solution could be derived through the coupling of the Einstein equations with nonlinear electrodynamics. Importantly, the authors highlighted that the solution is not always regular, outlining the necessary conditions for its regularity. Additionally, they conducted an in-depth analysis of the thermodynamics associated with this solution, establishing both the form of the Smarr formula and the first law of thermodynamics in this context. This comprehensive exploration provides valuable insights into the interplay between quintessence, nonlinear electrodynamics, and the properties of black hole solutions. The examination of critical phenomena in the context of Anti-de Sitter (AdS) black holes has been a focal point in various of scholarly works, each making valuable contributions to the expanding comprehension of this intricate field [19–23]. Extensive research is ongoing to comprehend phase transitions in quintessential black holes from diverse perspectives. The existence of a dark sector has prompted an examination into the thermodynamics concerning both charged and regular black holes, as explored in previous studies [24,25].

This research extensively explores the thermodynamic characteristics and critical phenomena exhibited by rotating regular AdS black holes within different theoretical frameworks. The paper is organized as follows: In Section 2, our focus shifts to the examination of rotating Bardeen black holes. We conduct a detailed analysis to understand how the charge parameter in nonlinear electrodynamics affects critical phenomena. Furthermore, we employ a precise calculation method to accurately determine the critical point associated with these rotating black holes. Section 3 is dedicated to computing and formulating the analytical expression for critical

point in Kerr Hayward AdS black holes. It also involves analyzing the phase transitions of this particular category of AdS black holes. We explore the impact of thermal fluctuations on the stability of Kerr-Hayward-AdS. Section 4 delves into the exploration of black holes characterized by a small horizon radius. Within this section, our research is dedicated to formulating an approximate method for deriving analytical expressions of critical points specific to these black holes when subjected to the influence of dark energy. Moving to Section 5, our attention is directed toward studying the impact of dark energy on black holes with a large horizon radius. Here, we utilize an approximate approach to establish analytical expressions for critical points, providing insights into the interplay between dark energy and black hole properties. In Section 6, we explore the influence of dark energy on the phase transitions of rotating Bardeen-AdS black holes. This involves a comprehensive analysis of various critical behaviors, contributing to a deeper understanding of the complex interactions at play. Finally, Section 7 serves as a pivotal integration point, where we consolidate the outcomes obtained from the preceding sections. This structured approach allows for a systematic exploration of the diverse aspects of Bardeen-AdS black holes, enriching our understanding of their thermodynamic properties and critical behaviors across different scenarios.

2 Unveiling key dynamics: Critical phenomena of rotating Bardeen-AdS black holes

The derivation of the line element governing the rotation of Bardeen-AdS black holes is established in connection with a cosmological constant, as explained in Ref. [26],

$$ds^{2} = \frac{-\Delta_{r}}{\Sigma} \left(dt - \frac{a\sin^{2}\theta}{E} d\phi \right)^{2} + \frac{\Sigma}{\Delta_{r}} dr^{2} + \frac{\Sigma}{\Delta_{\theta}} d\theta^{2} + \frac{\Delta_{\theta} \sin^{2}\theta}{\Sigma} \left(adt - \frac{r^{2} + a^{2}}{E} d\phi \right)^{2}, \quad (1)$$

where

$$\Delta_r = -2mr \left(\frac{r^2}{g^2 + r^2}\right)^{3/2} + \left(a^2 + r^2\right) \left(1 + \frac{8}{3}P\pi r^2\right). \tag{2}$$

In this context, g symbolizes the charge of nonlinear electrodynamics, m stands for the mass parameter, and a represents the rotational parameters of the black hole,

with

$$r = \frac{\sqrt{3S - 8a^2P\pi S - 3a^2\pi}}{\sqrt{3\pi}}, \qquad j = \frac{am}{\Xi^2}, \qquad \Xi = \frac{3 - 8a^2P\pi}{3}.$$
 (3)

Using the previously obtained expression for the horizon radius derived from the entropy formula of a rotating Bardeen-AdS black hole, and incorporating it into the equation for angular momentum, we obtain the following equation,

$$j = \frac{aS(3+8PS)\left(-3\left(g^2\pi + S\right) + a^2\pi(3+8PS)\right)^{3/2}}{2\sqrt{3\pi}\sqrt{3S - a^2\pi(3+8PS)}\left(-3S + a^2\pi(3+8PS)\right)^{3/2}}.$$
(4)

By using Eq. 3 and incorporating the derived expression for a(P, S, g) from Eq. 4 into the term $\frac{\Delta'_r}{4\pi(a^2+r^2)}$, we obtain the following expression representing the Hawking temperature,

$$T = \frac{t_1 + t_2 + t_3}{4B\sqrt{3\pi}S\sqrt{3B^2S - A^2\pi(3 + 8PS)}\left(-3B^2\left(g^2\pi + S\right) + A^2\pi(3 + 8PS)\right)}.$$
 (5)

Obtaining an analytical expression for the critical point involves solving a system of equations derived from the critical condition,

$$\left. \frac{\partial T}{\partial S} \right|_{P,q,j} = \left. \frac{\partial^2 T}{\partial S^2} \right|_{P,q,j} = 0,$$

which reduces to polynomial equations of degree greater than five with arbitrary coefficients in S. This makes exact resolution impossible without resorting to approximations. In our approach, we used the Taylor series to express the angular momentum j and truncated the series at the second order to make the mathematical problem tractable. This approximation is necessary to effectively address the problem of determining the critical point.

After a rigorous calculation, we derive the analytical expression for the critical point of rotating Bardeen-AdS black holes as follows.

$$P_{c} = \left(24g^{2} \left(179g^{4} + 435j^{2}\right) \pi^{3} P_{1} + P_{2} + P_{3} - \left(648 \ 2^{2/3} \left(17g^{4} - 30j^{2}\right)^{4} \pi^{8} + P_{4} + P_{5} - P_{6}\right) \gamma_{1} - 3\left(450 \ 2^{1/3} \left(17g^{5} - 30gj^{2}\right)^{2} \pi^{5} + P_{7}\right) \gamma_{0}^{1/3} \gamma_{1}^{3/2}\right) / \left(407040g^{10} \pi^{5} \gamma_{0}^{2/3} \gamma_{1}\right),$$

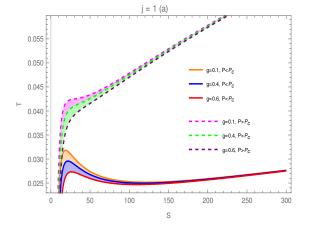
$$S_{c} = \frac{1}{2} \left(9g^{2} \pi + \sqrt{\gamma_{1}} + \sqrt{\gamma_{2}}\right),$$
(6)

with γ_0 , γ_1 , and γ_2 represented in relation to j and g (see Appendix).

To verify the accuracy of the analytical approximations derived in this study, we substituted j=0 into our results and compared them with the outcomes obtained in Ref. [27] for a non-rotating Bardeen-AdS black hole. Using relative deviation, we observed $|\Delta T_c| = 0.35\%$ and $|\Delta P_c| = 0.86\%$. This substantiates the robust validity of the approximate expressions obtained.

To evaluate the influence of the nonlinear electrodynamics charge on phase transitions, we generate graphs illustrating the relationship between temperature (T) and entropy (S), as well as Gibbs free energy (G) plotted against temperature (T). To carry out this analysis, we utilize Eq. 5 and incorporate the provided expression for G.

$$G = \frac{6j^2\pi^2S \left(4g^2\pi + S\right) + \left(g^2\pi + S\right)^4 \left(3 + 8PS\right)}{6\sqrt{\pi}S \left(g^2\pi + S\right)^{5/2}} - TS.$$
 (7)



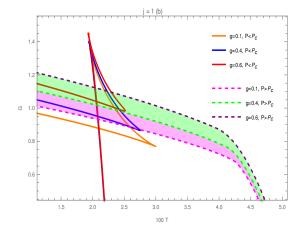


Figure 1: Graph (a): Temperature vs. entropy and graph (b): Gibbs free energy vs. temperature for varied g in rotating Bardeen-AdS black holes.

Graph (a) portrays the fluctuation of temperature with respect to entropy for $P < P_c$. The plot demonstrates oscillatory behavior that diminishes for $P > P_c$. The extremum points shift towards higher temperature values as the nonlinear electromagnetic charge decreases. Graph (b) visually represents the changes in Gibbs free energy as a function of temperature. This distinctive swallowtail pattern becomes evident when the pressure P is below the critical level, showcasing fluctuations. As the pressure surpasses the critical point, the swallowtail effect diminishes. Additionally, the introduction of a higher nonlinear electromagnetic charge g not only influences the intersection point but also causes a shift in the minimal temperature T_{min} towards higher values, accompanied by an increase in Gibbs free energy.

3 Analytical aspects of rotating Hayward-AdS black holes

We derived the thermodynamic quantities from the line element outlined in Ref. [28]. The expression for $\Delta(r)$ is formulated in terms of a, M, and g_h , where a a signifies the rotating parameter, M stands for the mass parameter, and g_h indicates the charge associated with non-linear electrodynamics,

$$\Delta_r = \left(a^2 + r^2\right) \left(1 + \frac{8}{3}P\pi r^2\right) - \frac{2Mr^4}{r^3 + g_h^3}.$$
 (8)

By applying the formula represented as $\frac{\Delta'r}{4\pi(a^2+r^2)}$, we express the representation of the Hawking temperature associated with Hayward AdS black holes as follow.

$$T = r \left(3 + 8a^{2}P\pi + 16P\pi r^{2} - \frac{2(a^{2} + r^{2})(3 + 8P\pi r^{2})}{r^{2}} + \frac{3r(a^{2} + r^{2})(3 + 8P\pi r^{2})}{2(r^{3} + g_{h}^{3})} \right)$$

$$/(6\pi (a^{2} + r^{2})).$$

$$(9)$$

In determining the entropy corrections due to thermal fluctuations, we base our calculations on the canonical partition function.

$$Z(\beta) = \int_0^\infty \sigma(E) \exp^{-\beta E} dE, \qquad (10)$$

the symbol $\sigma(E)$ denotes the quantum density of the system. By applying the inverse Laplace transformation, we derive the density of states,

$$\sigma(E) = \frac{-i}{2\pi} \int_{c-i\infty}^{c+i\infty} Z(\beta) \exp^{\beta E} d\beta, \qquad (11)$$

with S_0 denoting the corrected entropy, it is represented as,

$$S_0 = \beta \mathbf{E} + \mathbf{Log}[Z]. \tag{12}$$

After thorough and rigorous calculation, the formulation of the density of states is derived as follows,

$$\sigma(E) = \frac{-ie^S}{2\pi} \int_{c-i\infty}^{c+i\infty} \exp\frac{(\beta - c)^2}{2} \frac{d^2 S_0}{d^2 \beta} d\beta.$$
 (13)

After simplifying the calculations, the corrected entropy is expressed as a function of temperature, entropy, and corrected parameters,

$$S_0 = -\beta \operatorname{Log}\left(T^2 S\right) + \frac{\beta_0}{S} + S. \tag{14}$$

By substituting the content of Eq. 9 into Eq. 14, we formulate a modified expression. Setting the value of β_0 to 0 yields the resulting expression,

$$S_{0} = -\beta \operatorname{Log}\left(-\frac{\left(a^{2}r^{3}\left(-3 + 8P\pi r^{2}\right) + 3\left(r^{5} + 8P\pi r^{7}\right) - 2\left(3r^{2} + a^{2}\left(6 + 8P\pi r^{2}\right)\right)g_{h}^{3}\right)^{2}}{48\pi\left(-3 + 8a^{2}P\pi\right)r^{2}\left(a^{2} + r^{2}\right)\left(r^{3} + g_{h}^{3}\right)^{2}}\right) + \frac{3\pi\left(a^{2} + r^{2}\right)}{3 - 8a^{2}P\pi}.$$
(15)

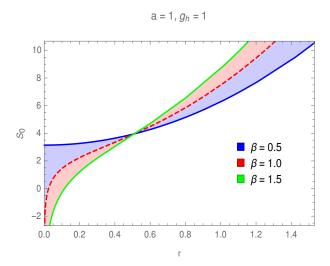


Figure 2: Dependence of corrected entropy on r for different values of corrected parameter.

The graphical representation delineates the fluctuations in both corrected and uncorrected entropy. Particularly noteworthy is the consistent observation that at equilibrium ($\beta = 0$), entropy not only retains a positive value but also exhibits a continuous and incremental rise. This trend aligns seamlessly with the underlying principles of the second law of black hole thermodynamics, which stipulates a perpetual increase in black hole entropy. Nevertheless, as the correction parameter β diverges from zero, smaller black holes tend to display a proclivity for negative entropy. This tendency becomes notably more pronounced with elevated β values. Additionally, for larger horizon radius, the corrected entropy consistently takes on positive values, resembling the pattern seen in uncorrected entropy. This discovery holds noteworthy implications, highlighting the considerable influence of thermal fluctuations on the thermodynamics of smaller black holes.

To derive and analytically express the critical point of the Kerr Hayward-AdS black hole, we follow a specific methodology outlined in two distinct cases. The first case pertains to a simplified scenario where the angular momentum parameter (a) is set to zero, and the second case deals with a more complex situation where the angular momentum parameter differs from zero.

For the case where a = 0, the Hawking temperature is formulated as follows:

$$T = \frac{r^3 + 8P\pi r^5 - 2g_h^3}{4\pi r^4 + 4\pi r g_h^3}. (16)$$

By applying the critical condition $\frac{\partial T}{\partial r}|_{j,g_h,P} = \frac{\partial^2 T}{\partial r^2}|_{j,g_h,P}$, the analytical expression for the critical point can be expressed as follows:

$$P_{c} = \frac{3(57 - 23\sqrt{6})(14 + 6\sqrt{6})^{1/3}}{800\pi g_{h}^{2}},$$

$$v_{c} = 2(14 + 6\sqrt{6})^{1/3}g_{h},$$

$$T_{c} = \frac{(5 - 2\sqrt{6})(7 + 3\sqrt{6})^{2/3}}{42^{1/3}\pi g_{h}}.$$
(17)

We discover that the equation of state suggests a universal ratio, given by:

$$\rho_h = \frac{P_c v_c}{T_c} = \frac{-3\sqrt{6} + 27}{50} \simeq 0.393,$$

this ratio differs from the universal one identified for Van der Waals fluids, where $\rho = 0.375$.

In the scenario where angular momentum is non-zero, in the small limit of j, we obtain the expressions for r and a from the equations of entropy (S) and angular momentum (j) of the Hayward-AdS black hole as indicated below,

$$r = \frac{\sqrt{3 - 8a^2P\pi}\sqrt{3a^2\pi - 3S + 8a^2P\pi S}}{\sqrt{3\pi}\sqrt{-3 + 8a^2P\pi}},$$
(18)

$$a = \frac{6j\sqrt{\pi}S}{(3+8PS)\left(S^{3/2} + \pi^{3/2}g_b^3\right)} + O\left(j^2\right). \tag{19}$$

By replacing the expressions from Eq. 18 and Eq. 19 into Eq. 9, we derive.

$$T = \left(-2\pi^{6}g_{h}^{12}\left(3 + 8PS\right) + \pi^{9/2}g_{h}^{9}S^{3/2}\left(-15 - 16PS + 64P^{2}S^{2}\right) + S^{4}\left(3 + 8PS\right)\right)$$

$$\left(-6j^{2}\pi^{2} + S^{2} + 8PS^{3}\right) + 3\pi^{3}g_{h}^{6}S\left(-12j^{2}\pi^{2} + S^{2}\left(-3 + 16PS + 64P^{2}S^{2}\right)\right) +$$

$$\pi^{3/2}g_{h}^{3}S^{5/2}\left(-12j^{2}\pi^{2}\left(9 + 16PS\right) + S^{2}\left(3 + 80PS + 192P^{2}S^{2}\right)\right)\right) / \left(4\sqrt{\pi}\sqrt{S}\right)$$

$$\left(3 + 8PS\right)\left(\pi^{3/2}g_{h}^{3} + S^{3/2}\right)^{4}\right). \tag{20}$$

By applying the critical condition $\frac{\partial T}{\partial S}|_{j,g_h,P} = \frac{\partial^2 T}{\partial^2 S}|_{j,g_h,P}$, and adopting the same procedure used in Section 2, after simplifying, we obtain the following derivation.

$$P_{c} = \left(\xi_{1} + c_{2} \left(\xi_{4} - \xi_{5} - \xi_{6}\right) + 18c_{1}^{2/3}c_{2} \left(\xi_{7} + \xi_{8}\right) + 3c_{1}^{1/3}\sqrt{c_{2}} \left(10\pi^{3}g_{h}^{6}\left(\xi_{2} + \xi_{3}\right) + 3c_{2}\right)\right) \left(\xi_{9} + \xi_{10}\right)\right) / \xi_{11},$$

$$S_{c} = \frac{1}{2} \left(\sqrt{c_{2}} + \sqrt{c_{3}}\right),$$
(21)

with $\xi_1, \xi_2, \xi_3, \dots, \xi_{10}$ and c_1, c_2, c_3 are expressed in terms of g_h and j (see Appendix).

To analyze the phase transition of Kerr-Hayward AdS black holes, we utilize Eq. 20 to plot T as a function of S. Additionally, we employ the formula $C = T \frac{dS}{dT}$ to graph the heat capacity as a function of entropy S.

The expression for Gibbs energy is determined by employing the equation G = m - TS, along with Eq. 8 and Eq. 20, where m denotes the physical mass of Kerr-Hayward -Ads black holes. The mass parameter is established by imposing the condition $\Delta(r) = 0$.

$$G = -TS + \left(\pi^{9/2}g_h^9 \left(3 + 8PS\right) + 3\pi^3 g_h^6 S^{3/2} \left(3 + 8PS\right) + S^{5/2} \left(6j^2\pi^2 + (3 + 8PS)\right)\right) S^2 + 3\pi^{3/2}g_h^3 S \left(8j^2\pi^2 + S^2 \left(3 + 8PS\right)\right)\right) / \left(6\sqrt{\pi}S \left(\pi^{3/2}g_h^3 + S^{3/2}\right)^2\right).$$
(22)

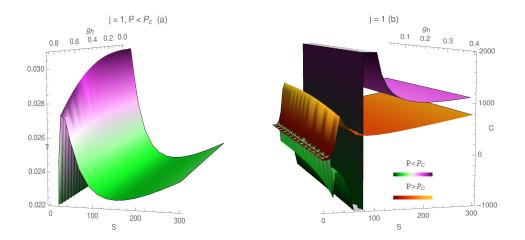


Figure 3: Graph (a): Temperature vs. entropy, Graph (b): Heat capacity vs. entropy.

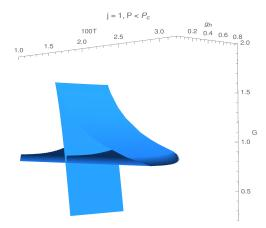


Figure 4: Gibbs energy vs. temperature for non-linear electrodynamics charge.

The description of the temperature-entropy plot (Figure. 3, graph (a)) under conditions where pressure P is below the critical pressure shows oscillatory behavior. Two extreme points move towards higher temperatures as the charge of the non-linear electrodynamics decreases, creating a concave curve with $g_h = 0$ symbolizing the peak. For graph (b): Below the critical pressure, a negative slope indicates an intermediate black hole branch with negative heat capacity, suggesting system instability. Heat capacity divergence signals an ongoing phase transition. Above the critical pressure, no phase transition occurs, restoring system stability. The Gibbs diagram (Figure. 4) reveals a distinct swallowtail pattern, noticeable when the pressure is less than the critical pressure. As the charge of the non-linear electrodynamics rises, the intersection point shifts towards higher G and lower T.

| rotating Bardeen-AdS black holes | | | | | | | | |
|----------------------------------|----------|-----------|----------|----------|--|--|--|--|
| g | P_c | S_c | T_c | G_c | | | | |
| 0.3 | 0.010547 | 6.069231 | 0.076726 | 0.405439 | | | | |
| 0.5 | 0.004516 | 12.931001 | 0.049630 | 0.639051 | | | | |
| 0.8 | 0.001822 | 31.279590 | 0.031444 | 1.012064 | | | | |
| rotating Hayward-AdS black holes | | | | | | | | |
| g_h | P_c | S_c | T_c | G_c | | | | |
| 0.3 | 0.013261 | 6.186845 | 0.091029 | 0.304038 | | | | |
| 0.5 | 0.006796 | 12.029185 | 0.064658 | 0.435181 | | | | |
| 0.8 | 0.003441 | 23.736345 | 0.045291 | 0.640423 | | | | |

Table 1: Critical thermodynamic quantities for rotating Bardeen and Hayward-AdS black holes.

Table 1 presents numerical results for various critical thermodynamic quantities for rotating Bardeen-AdS black holes and rotating Hayward-AdS black holes. The aim is to compare the effect of the non-linear electrodynamics charge on these properties. It has been observed that the non-linear electrodynamics charge exerts a similar influence on both rotating Bardeen-AdS and rotating Hayward-AdS black holes. An increase in the charge values results in a decrease in the critical temperature and critical pressure. Conversely, the critical entropy and Gibbs energy increase in value, indicating that a higher non-linear electrodynamics charge leads to a lower phase transition temperature and a larger associated entropy.

4 Analytical expression for critical point in small horizon radius of rotating Bardeen AdS black holes with dark energy

We derive the thermodynamic properties of rotating Bardeen-AdS black holes that include a quintessence field, referencing [11], and [29]. Our primary objective is to investigate the influence of dark energy on the critical phenomena exhibited by these black holes. This section is specifically dedicated to exploring the dynamics of rotating Bardeen-AdS black holes enriched with dark energy, with a particular emphasis on situations where the horizon radius is characterized by small values.

$$\Delta_r = -2mr \left(\frac{r^2}{b^2 + r^2}\right)^{3/2} + \left(a^2 + r^2\right) \left(1 + \frac{8}{3}P\pi r^2\right) - r^{-1-3\omega}\alpha,\tag{23}$$

in this context, b is indicative of the nonlinear electromagnetic charge, while ω represents the state parameter for quintessence. Additionally, α is used to characterize the intensity of the quintessence.

Deriving an analytical expression for the critical point involves solving a set of equations derived from the critical condition, $\frac{\partial T}{\partial S}|_{P,b,j,\omega,\alpha} = \frac{\partial^2 T}{\partial^2 S}|_{P,j,b,\omega,\alpha} = 0$, which relies on the Hawking temperature derived from $\frac{\Delta'_r}{4\pi(a^2+r^2)}$. These equations are of arbitrary order due to the presence of the $-1-3\omega$ term in the expression for Δ_r , making exact resolution unfeasible without employing approximations. To tackle this mathematical challenge, we used the Taylor series to represent the horizon, as depicted in Eq.23. This approximation was necessary to

effectively address the task of determining the critical point. Truncating the series at the first order provided results comparable to those of rotating Bardeen-AdS black holes, when we set additional parameters to zero. Moreover, restricting the order to 1 helps avoid unnecessary complexities.

$$r^{-1-3\omega} = 2 + 3\omega - r(1+3\omega) + O(r-1)^2,$$
(24)

$$m = \frac{(b^2 + r^2)(3a^2 + 3r^2 + 8a^2P\pi r^2 + 8P\pi r^4 - 6\alpha + 3r\alpha - 9\alpha\omega + 9r\alpha\omega)}{6r^3\sqrt{\frac{r^2}{b^2 + r^2}}},$$
 (25)

the mass parameter m is deduced from Eq. 23 when $\Delta_r = 0$, and this derivation involves applying the Taylor expansion to Eq. 24, which describes the horizon radius.

$$T = \frac{-a^{2} (3r^{2} - 8P\pi r^{4} + 4b^{2} (3 + 4P\pi r^{2})) + 3 (b^{2} (-2r^{2} + 4\alpha(2 + 3\omega) - 3r(\alpha + 3\alpha\omega)))}{12\pi r (a^{2} + r^{2}) (b^{2} + r^{2})} + \frac{3r^{2} (r^{2} + 8P\pi r^{4} + \alpha(2 + 3\omega))}{12\pi r (a^{2} + r^{2}) (b^{2} + r^{2})}.$$
(26)

In the small limit of j, we represent the parameter of angular momentum a as,

$$a = \frac{6j\sqrt{\pi}S^{3/2}\sqrt{\frac{S}{b^2\pi + S}}}{(b^2\pi + S)\left(3S + 8PS^2 - 6\pi\alpha + 3\sqrt{\pi}\sqrt{S}\alpha - 9\pi\alpha\omega + 9\sqrt{\pi}\sqrt{S}\alpha\omega\right)} + O(j)^2.$$
 (27)

Through the replacement of the expressions from Eq. 3 and Eq. 27 into Eq. 25, and subsequent application of the critical condition, we obtained an approximate analytical expression for the critical point through a sequence of simplifications.

$$P_{c} = \frac{(P_{1S} + P_{2S} + P_{3S} + P_{4S})}{(8480b^{10}\pi^{5})},$$

$$S_{c} = \frac{1}{4} \left(18b^{2}\pi - 12\pi\alpha - 18\pi\alpha\omega \right) + \frac{\sqrt{\lambda_{4}}}{2} + \frac{\sqrt{\lambda_{5}}}{2},$$
(28)

with P_{1s} , P_{2S} , P_{3S} , P_{4S} , λ_4 , λ_5 expressed in terms of b, j, ω , α (see the appendix).

Setting the quintessential state parameter $\omega = 0$ and the intensity of quintessence $\alpha = 0$ yields identical results to those obtained in Section 2.

5 Deriving analytical expression for critical point of rotating Bardeen-AdS black holes with dark energy at large horizon radius

In this particular section, our attention is directed towards analyzing how quintessence affects large rotating Bardeen-AdS black holes. This involves deriving the analytical expression for the critical point. We employ the same procedure as in Section 4 To facilitate this analysis,

we adopt the following approximation, with n is the convergence value of the event horizon radius.

$$r^{-1-3\omega} = n^{-2-3\omega}(-r(1+3\omega) + n(2+3\omega)) + O(r-n)^2.$$
 (29)

The earlier equation is derived by employing the Taylor series expansion of the horizon radius expression, which converges towards values much larger than 1. We limited the Taylor expansion to the first order for the same reasons discussed in Section 4,

$$m = \frac{n^{-2-3\omega} \left(a^2 n^{2+3\omega} \left(3 + 8P\pi r^2\right) + n^{2+3\omega} r^2 \left(3 + 8P\pi r^2\right) + 3r\alpha(1+3\omega) - 3n\alpha(2+3\omega)\right)}{6r \left(\frac{r^2}{b^2 + r^2}\right)^{3/2}},$$
(30)

the mass parameter of a rotating Bardeen-AdS black hole with dark energy, particularly for large values of the horizon radius, is derived through the utilization of a specific Eq. 23.

$$T = \left(-a^2 n^{2+3\omega} \left(3r^2 - 8P\pi r^4 + 4b^2 \left(3 + 4P\pi r^2\right)\right) + 3\left(nr^2 \left(n^{1+3\omega} \left(r^2 + 8P\pi r^4\right) + \alpha(2+3\omega)\right) + b^2 \left(-2n^{2+3\omega} r^2 - 3r\alpha(1+3\omega) + 4n\alpha(2+3\omega)\right)\right)\right) / \left(12\pi r \left(a^2 + r^2\right) \left(b^2 + r^2\right) n^{-2-3\omega}\right).$$
(31)

In order to determine the critical point, the angular momentum parameter must be expressed in relation to P and S as follows,

$$a = \frac{6jn^{2+3\omega}\sqrt{\pi}\sqrt{S}\left(\frac{S}{b^2\pi + S}\right)^{3/2}}{n^{2+3\omega}S(3+8PS) + 3\sqrt{\pi}\sqrt{S}\alpha(1+3\omega) - 3n\pi\alpha(2+3\omega)} + O(j)^2.$$
 (32)

Substituting Eq. 3 and Eq. 32 into Eq. 31 while adopting the identical critical condition from Section 4, we provide approximate analytical expression for the critical point of rotating Bardeen-Ads black holes enveloped by quintessence. This analysis is specifically tailored for scenarios characterized by significantly large values of the horizon radius.

$$P_{c} = \frac{n^{-1-3\omega}(P_{1L} + P_{2L} + P_{3L})}{8480b^{10}\pi^{5}},$$

$$S_{c} = \frac{3}{2}n^{-1-3\omega}\pi \left(3b^{2}n^{1+3\omega} - 2\alpha - 3\alpha\omega\right) + \frac{\sqrt{\beta_{3}}}{2} + \frac{\sqrt{\beta_{4}}}{2},$$
(33)

with β_1 , β_2 , β_3 , and β_4 are formulated in relation to j, n, g, ω , b, and α (see Appendix).

By setting the external parameters of the quintessence field $\alpha = 0$ and $\omega = 0$, we observe consistent results with those detailed in Section 2.

The calculations are presented in Table 2. It has been observed that, for different values of the equation of state parameter ω , an increase in the charge of nonlinear electrodynamics results in a decrease in the critical temperature and pressure, while the critical entropy and Gibbs free energy increase. Furthermore, when the value of b is fixed, it is noted that as ωq increases, the critical pressure and temperature increase, whereas the critical entropy and Gibbs free energy decrease.

| ω | b | P_c | S_c | T_c | G_c |
|----------------|-----|----------|-----------|----------|----------|
| -1 | 0.3 | 0.008177 | 7.707532 | 0.067932 | 0.373279 |
| | 0.5 | 0.003956 | 14.931977 | 0.046928 | 0.579808 |
| | 0.8 | 0.001720 | 33.432813 | 0.030801 | 0.931611 |
| $\frac{-2}{3}$ | 0.3 | 0.010987 | 5.724030 | 0.078332 | 0.349819 |
| | 0.5 | 0.004639 | 12.345093 | 0.050434 | 0.577299 |
| | 0.8 | 0.001844 | 30.627317 | 0.031718 | 0.949997 |
| $\frac{-1}{3}$ | 0.3 | 0.017056 | 3.645610 | 0.096235 | 0.308704 |
| | 0.5 | 0.005760 | 9.18768 | 0.055334 | 0.564254 |
| | 0.8 | 0.001996 | 27.566450 | 0.032755 | 0.966299 |

Table 2: Critical thermodynamic quantities for different values of ω and b with $j = \alpha = 0.1$.

6 Critical behaviors of rotating bardeen AdS black holes with quintessence field

In this section, we use the following expressions for temperature and Gibbs free energy. These expressions are general and applicable to both small and large values of the horizon radius for rotating Bardeen-AdS black holes with dark energy. We graph the relationship between temperature T and entropy S, with a specific emphasis on scenarios where the pressure is below the critical pressure.

$$T = \frac{S^{-2-\frac{3\omega}{2}} \left(12j^2\pi^2 S^{4+3\omega} \left(b^2\pi + S\right) \left(-S^2T_2 + b^2\pi ST_3 + b^4T_4\right) + T_1T_5\right)}{4\sqrt{\pi} \left(b^2\pi + S\right) T_5}.$$
 (34)

 T_1, T_2, T_3, T_4, T_5 are expressed in terms of j, b, α, ω, P , and S. Further details can be found in the Appendix.

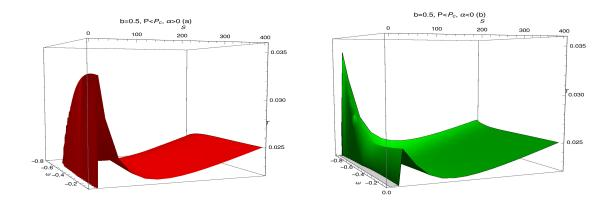


Figure 5: Exploring the impact of quintessence intensity on temperature: Positive values (graph a) and negative values (graph b).

The temperature-versus-entropy plot, considering diverse values of the quintessential state parameter ω , reveals oscillatory patterns for both positive and negative quintessence intensities when the pressure is below the critical point. Specifically, in instances of positive quintessence intensity, the extrema indicate a decreasing trend in temperature as ω decreases, shaping a concave function. Conversely, for negative quintessence intensity, the extrema show an increase

as ω values decrease, illustrating a convex function.

$$G = -ST + \frac{S^{-\frac{3}{2}(2+\omega)} \left(36j^2\pi^2 S^{5+3\omega} \left(SM_2 + M_3\right) + \left(b^2\pi + S\right)^3 M_1 M_4\right)}{36\sqrt{\pi} \sqrt{\frac{S}{b^2\pi + S}} \left(b^2\pi + S\right)^3 M_4}.$$
 (35)

The expressions for M_1 , M_2 , M_3 , and M_4 are presented using the variables j, b, α , ω , and S. Further details can be found in the Appendix.

To assess the impact of the quintessence field on critical behaviors, we represent the Gibbs free energy as a function of entropy in the subsequent plots.

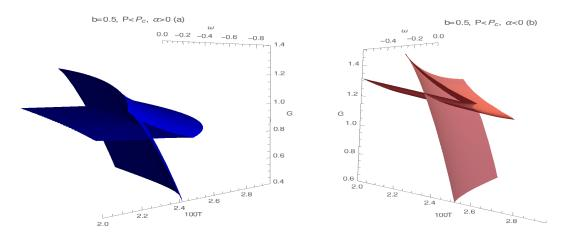


Figure 6: Gibbs free energy in relation to temperature for various ω values: Positive α (graph a) and negative α scenarios (graph b).

The plotted graph illustrating Gibbs energy as a function of temperature, considering different ω values and various quintessence intensity scenarios α , showcases distinctive swallowtail patterns when the pressure is below the critical threshold. Positive α values lead to the intersection point and minimal temperature shifting towards higher temperature and Gibbs free energy values as ω increases, delineating a concave pattern. Conversely, for negative α values, the intersection point and minimal temperature shift towards lower Gibbs free energy and higher temperature values as ω increases, revealing a convex pattern.

7 Conclusion

In this recent research, we focus centrally on the notable impact of dark energy on determining the critical point of rotating Bardeen-AdS black holes. We formulated approximate analytical expressions to establish a nuanced relationship between the parameters and thermodynamic features of rotating Bardeen-AdS black holes and those linked to the dark sector. Rigorous validation procedures were implemented to verify the accuracy and reliability of the derived expressions for critical point. This research offers a deeper understanding of the thermodynamic characteristics of rotating Hayward-AdS black holes, highlighting how thermal fluctuations affect both large and small black holes. The introduction of a non-zero correction parameter leads smaller black holes to favor negative entropy. We derive analytical expressions for critical point, exploring the impact of the non-linear electrodynamics charge on the phase transition

of rotating Hayward-AdS black holes. Moreover, our examination extends to unraveling the influence of the charge of nonlinear electrodynamics on the critical phenomena of rotating regular AdS black holes.

By illustrating diverse critical behaviors, we underscore the impact of quintessence intensity on the dynamics of phase transitions. Specifically, when quintessence intensity is positive, the extrema imply a decline in temperature as ω decreases, forming a concave function. Conversely, under negative quintessence intensity, the extrema suggest an increase as ω values decrease, depicting a convex function. Additionally, our findings revealed that positive α values prompt the intersection point and minimal temperature to shift towards higher temperature and Gibbs free energy values as ω increases, resulting in a concave pattern. Conversely, negative α values cause the intersection point and minimal temperature to move towards lower Gibbs free energy and higher temperature values as ω increases, unveiling a convex pattern. The novel findings emerging from this study underscore the substantial influence exerted by the quintessence field on the critical phenomena observed in rotating Bardeen-AdS black holes.

Acknowledgements

The authors would like to thank the anonymous referee for interesting comments and suggestions which motivated us to prepare a well-improved revised version.

References

- [1] J. M. Bardeen: Proc. Int. Conf. GR5, Tbilisi 174, (1968).
- [2] E. Ayon-Beato, A. Garcia, The Bardeen Model as a Nonlinear Magnetic Monopole, Phys. Lett. B 493 (2000) 149-152.
- [3] H. C. D. Lima and L. C. B. Crispino, "Tidal forces in the charged Hayward black hole spacetime", Int. J. Mod. Phys. D 29, no.11, 2041014 (2020).
- [4] M. A. A. Paula, L. C. S. Leite and L. C. B. Crispino, Electrically charged black holes in linear and nonlinear electrody-namics: Geodesic analysis and scalar absorption, Phys. Rev. D 102, no.10, 104033 (2020).
- [5] C. F. B. Macedo, E. S. de Oliveira and L. C. B. Crispino, Scattering by regular black holes: Planar massless scalar waves impinging upon a Bardeen black hole, Phys. Rev. D 92, no.2, 024012 (2015).
- [6] C. F. B. Macedo and L. C. B. Crispino, Absorption of planar massless scalar waves by Bardeen regular black holes, Phys. Rev. D 90, no.6, 064001 (2014).
- [7] C. F. B. Macedo, L. C. B. Crispino and E. S. de Oliveira, Scalar waves in regular Bardeen black holes: Scattering, absorption and quasinormal modes, Int. J. Mod. Phys. D 25, no.09, 1641008 (2016).
- [8] Belinchón, J. A. (2017). Nonlinear electrodynamics: a new framework for fundamental theories in particle physics, gravitation, and cosmology. International Journal of Geometric Methods in Modern Physics, 14(08), 1750136.
- [9] Hayward, S. A. (2006). Formation and evaporation of regular black holes. Physical Review Letters, 96(3), 031103.
- [10] Ayón-Beato, E., & García, A. (2000). Regular black hole in general relativity coupled to nonlinear electrodynamics. Physical Review Letters, 80(23), 5056.
- [11] V. V. Kiselev, Quintessence and black holes, Class. Quant. Grav. 20 (2003) 1187.
- [12] S. Chen, B. Wang, R. Su, Phys. Rev. 77, 124011 (2008).
- [13] Daassou, A., Benbrik, R.& Laassiri, H. Effect of cloud of strings and quintessence on a phase transition of charged rotating AdS black holes. Theor Math Phys 215,893-908(2023).
- [14] Mohamed Chabab, Samir Iraoui, Thermodynamic criticality of d-dimensional charged AdS black holes surrounded by quintessence with a cloud of strings background, Gen Relativ Gravit 52, 75 (2020).
- [15] S. W. Wei, Q. T. Man, H. Yu, Thermodynamic Geometry of Charged AdS Black Hole Surrounded by Quintessence, Commun. Theor. Phys. 69 (2018) 173.
- [16] Aritra Banerjee, Haiying Cai, Lavinia Heisenberg, Eoin Ó Colgáin, M. M. Sheikh-Jabbari, Tao Yang, Hubble sinks in the low-redshift swampland, Phys. Rev. D 103, 081305 (2021).
- [17] M. Saleh, B.B. Thomas, T.C. Kofane, Eur. Phys. J. C 78, 325 (2018).
- [18] Manuel E. Rodrigues, Marcos V. de S. Silva and Henrique A. Vieira, Phys.Rev.D 105, 8 (2022).
- [19] S. Chen, X. Liu, C. Liu, and J. Jing, Critical Behavior of Black Holes in an Einstein—Maxwell Gravity with a Conformal Anomaly, Chin. Phys. Lett. 30, 060401 (2013).
- [20] S.-W. Wei and Y.-X. Liu, Insight into the Microscopic Structure of an AdS Black Hole from Thermodynamical Phase Transition, Phys. Rev. D 91, 044018 (2015).
- [21] B. P. Dolan, Black holes and Boyle's law The thermodynamics of the cosmological constant, Mod. Phys. Lett. A 30, 1540002 (2015).
- [22] R. Zhao, H.-H. Zhao, M.-S. Ma, and L.-C. Zhang, Classical and Quantum Gravity Paper Phase transition and Clapeyron equation of black holes in higher dimensional AdS spacetime, Eur. Phys. J. C 73, 2645(2013).

- [23] J.-L. Zhang, R.-G. Cai, and H.-W. Yu, Phase transition and Thermodynamical geometry of Reissner-Nordström-AdS Black Holes in Extended Phase Space, Phys. Rev. D 91, 044028 (2015).
- [24] B. B. Thomas, M. Saleh, T. C. Kofane, Thermodynamics and phase transition of the Reissner-Nordstrom black hole surrounded by quintessence, Gen. Rel. Grav. 44 (2012).
- [25] H.Laassiri, A.Daassou, R.Benbrik, Responses of Small and Large Ads Black Holes to the Collective Influence of Quintessence and String Cloud ,arXiv:2312.08868.
- [26] M. S. Ali, S. G. Ghosh, Thermodynamics of rotating Bardeen black holes: Phase transitions and thermodynamics volume, Phys. Rev. D 99 (2019) 024015.
- [27] Sen Guo, Guan-Ru Li, Guo-Ping Li, Shadow thermodynamics of AdS black hole in regular spacetime, Chinese Phys. C 46 095101.
- [28] Adil Belhaj et al. Light Deflection by Rotating Regular Black Holes with a Cosmological Constant, arXiv:2204.10150 (2022).
- [29] Adil Belhaj, et al. Optical Shadows of Rotating Bardeen AdS Black Holes, Modern Physics Letters A (2022), 10.1142.

Appendix

Appendix A: Rotating Bardeen-AdS black holes

$$t_{1} = -2A^{4}\pi^{2}(1 + 4PS)(3 + 8PS)^{2},$$

$$t_{2} = -9B^{4}S(-2g^{2}\pi + S + 8PS^{2}),$$

$$t_{3} = 3A^{2}B^{2}\pi(3 + 8PS)(2g^{2}\pi + S(3 + 16PS)),$$

$$A = 6j\sqrt{\pi}\left(\frac{S}{g^{2}\pi + S}\right)^{3/2},$$

$$B = \sqrt{S}(3 + 8PS),$$

$$P_{1} = \left(36\ 2^{1/3}\left(17g^{4} - 30j^{2}\right)^{2}\pi^{4} + 15\left(37g^{4} + 48j^{2}\right)\pi^{2}\gamma_{0}^{1/3} + 2\ 2^{2/3}\gamma_{0}^{2/3}\right)\gamma_{0}^{1/3}\sqrt{\gamma_{1}},$$

$$P_2 = 6\gamma_0^{2/3}\gamma_1^{5/2} \left(25g^2\pi + 12\sqrt{\gamma_2}\right),\,$$

$$P_3 = 288g^4 \left(179g^4 + 435j^2\right)^2 \pi^6 \gamma_0^{2/3},$$

$$P_4 = 4 \ 2^{1/3} \gamma_0^{4/3} - 270 \ 2^{1/3} \left(17g^4 - 30j^2\right)^2 \pi^5 \gamma_0^{1/3} \left(44g^4\pi + 48j^2\pi + 5g^2\sqrt{\gamma_2}\right),$$

$$P_5 = 6\gamma_0^{2/3} \left(12 \left(1691g^8 + 9670g^4j^2 + 2700j^4 \right) \pi^4 + 12g^2 \left(1076g^4 + 2115j^2 \right) \pi^3 \sqrt{\gamma_2} - 25g^2 \pi \gamma_2^{3/2} \right) \eta^4 + 12g^2 \left(1076g^4 + 2115j^2 \right) \pi^3 \sqrt{\gamma_2} - 25g^2 \pi \gamma_2^{3/2} \right) \eta^4 + 12g^2 \left(1076g^4 + 2115j^2 \right) \pi^3 \sqrt{\gamma_2} - 25g^2 \pi \gamma_2^{3/2} \right) \eta^4 + 12g^2 \left(1076g^4 + 2115j^2 \right) \pi^3 \sqrt{\gamma_2} - 25g^2 \pi \gamma_2^{3/2} \right) \eta^4 + 12g^2 \left(1076g^4 + 2115j^2 \right) \pi^3 \sqrt{\gamma_2} - 25g^2 \pi \gamma_2^{3/2} \right) \eta^4 + 12g^2 \left(1076g^4 + 2115j^2 \right) \pi^3 \sqrt{\gamma_2} - 25g^2 \pi \gamma_2^{3/2} \right) \eta^4 + 12g^2 \left(1076g^4 + 2115j^2 \right) \pi^3 \sqrt{\gamma_2} - 25g^2 \pi \gamma_2^{3/2} \right) \eta^4 + 12g^2 \left(1076g^4 + 2115j^2 \right) \pi^3 \sqrt{\gamma_2} - 25g^2 \pi \gamma_2^{3/2} \right) \eta^4 + 12g^2 \left(1076g^4 + 2115j^2 \right) \pi^3 \sqrt{\gamma_2} - 25g^2 \pi \gamma_2^{3/2} \right) \eta^4 + 12g^2 \left(1076g^4 + 2115j^2 \right) \pi^3 \sqrt{\gamma_2} - 25g^2 \pi \gamma_2^{3/2} \right) \eta^4 + 12g^2 \left(1076g^4 + 2115j^2 \right) \pi^3 \sqrt{\gamma_2} - 25g^2 \pi \gamma_2^{3/2} \right) \eta^4 + 12g^2 \left(1076g^4 + 2115j^2 \right) \pi^3 \sqrt{\gamma_2} - 25g^2 \pi \gamma_2^{3/2} \right) \eta^4 + 12g^2 \left(1076g^4 + 2115j^2 \right) \eta^4 + 12g^2 \left(1076g^4 + 211$$

$$P_6 = 15 \ 2^{2/3} \pi \gamma_0 \left(44g^4 \pi + 48j^2 \pi + 5g^2 \sqrt{\gamma_2} \right),$$

$$P_7 = 25 \ 2^{2/3} g^2 \pi \gamma_0^{2/3} + 6 \gamma_0^{1/3} \left(29 g^2 \left(101 g^4 + 240 j^2 \right) \pi^3 + 10 \left(73 g^4 + 72 j^2 \right) \pi^2 \sqrt{\gamma_2} - 4 \gamma_2^{3/2} \right),$$

 γ_0 , γ_1 , γ_2 are represented in relation to 'j' and 'g' in the following expressions,

$$\gamma_0 = 54\pi^6 \left(4737g^{12} - 18930g^8j^2 + 63900g^4j^4 - 27000j^6 + 4\sqrt{5} \right)$$

$$\sqrt{-g^4 \left(21230g^{20} - 952893g^{16}j^2 + 2047500g^{12}j^4 + 275400g^8j^6 - 19926000g^4j^8 + 12150000j^{10} \right)}$$

$$\gamma_{1} = \frac{18\ 2^{1/3}\left(17g^{4} - 30j^{2}\right)^{2}\pi^{4} + 30\left(11g^{4} + 12j^{2}\right)\pi^{2}\gamma_{0}^{1/3} + 2^{2/3}\gamma_{0}^{2/3}}{6\gamma_{0}^{1/3}},$$

$$\gamma_{2} = \frac{\left(-182^{1/3} \left(17 g^{4} - 30 j^{2}\right)^{2} \pi^{4} + 60 \left(11 g^{4} + 12 j^{2}\right) \pi^{2} \gamma_{0}^{1/3} - 2^{2/3} \gamma_{0}^{2/3}\right)}{6 \gamma_{0}^{1/3}} + \frac{24 g^{2} \left(179 g^{4} + 435 j^{2}\right) \pi^{3}}{6 \sqrt{\gamma_{1}}}.$$

Appendix B: Rotating Hayward-AdS black holes

$$\xi_1 = -28800\pi^6 c_1^{2/3} g_h^{12} - 18c_1^{2/3} c_2^{5/2} \left(16\sqrt{c_3} + 5\pi^{3/2} g_h^3 \right),$$

$$\xi_2 = 32 \ 2^{2/3} c_1^{2/3} + 2304 \ 2^{1/3} \pi^3 \left(15 j^2 \sqrt{\pi} + 28 g_h^3\right)^2,$$

$$\xi_3 = 3c_1^{1/3} \left(3840j^2\pi^2 + 8192\pi^{3/2}q_h^3 + 25\pi^3q_h^6\right).$$

$$\xi_4 = 16 \ 2^{1/3} c_1^{4/3} + 41472 \ 2^{2/3} \pi^6 \left(15 j^2 \sqrt{\pi} + 28 g_b^3\right)^4,$$

$$\begin{split} \xi_5 &= 3\ 2^{2/3} \pi^{3/2} c_1 \left(960 j^2 \sqrt{\pi} + \left(2048 + 15 \sqrt{c_3}\right) g_h^3\right), \\ \xi_6 &= 216\ 2^{1/3} \pi^{9/2} c_1^{1/3} \left(15 j^2 \sqrt{\pi} + 28 g_h^3\right)^2 \left(960 j^2 \sqrt{\pi} + \left(2048 + 15 \sqrt{c_3}\right) g_h^3\right), \\ \xi_7 &= 43200 j^4 \pi^4 + 5 \pi^{3/2} \left(38400 j^2 \pi^2 + 180 j^2 \pi^2 \sqrt{c_3} - c_3^{3/2}\right) g_h^3, \\ \xi_8 &= 3 \pi^3 \left(70656 + 375 j^2 \pi^2 + 560 \sqrt{c_3}\right) g_h^6 + 2400 \pi^{9/2} g_h^9, \\ \xi_9 &= 5\ 2^{2/3} \pi^{3/2} c_1^{2/3} g_h^3 + 360\ 2^{1/3} \pi^{9/2} g_h^3 \left(15 j^2 \sqrt{\pi} + 28 g_h^3\right)^2, \\ \xi_{10} &= c_1^{1/3} \left(-32 c_3^{3/2} - 480 \pi^3 g_h^6 + \sqrt{c_3} \left(5760 j^2 \pi^2 + 12288 \pi^{3/2} g_h^3 - 25 \pi^3 g_h^6\right)\right), \\ \xi_{11} &= 2160 \pi^{9/2} c_1^{2/3} c_2 g_h^9 \left(256 + 25 \pi^{3/2} g_h^3\right), \\ c_1 &= -108 \left(c_{11} + \sqrt{c_{11}^2 - 16 \pi^9} \left(15 j^2 \sqrt{\pi} + 28 g_h^3\right)^6\right), \\ c_{11} &= \left(13500 j^6 \pi^6 + 108000 j^4 \pi^{11/2} g_h^3 + 273600 j^2 \pi^5 g_h^6 + 223232 \pi^{9/2} g_h^9 - 25 \pi^6 g_h^{12}\right), \\ c_2 &= \frac{2^{2/3} c_1^{2/3} + 72\ 2^{1/3} \pi^3 \left(15 j^2 \sqrt{\pi} + 28 g_h^3\right)^2 + 24 c_1^{1/3} \left(15 j^2 \pi^2 + 32 \pi^{3/2} g_h^3\right)}{6 c_1^{1/3}}, \\ c_3 &= \frac{-120 \pi^3 c_1^{1/3} g_h^6 - \sqrt{c_2} \left(2^{2/3} c_1^{2/3} + 72\ 2^{1/3} \pi^3 \left(15 j^2 \sqrt{\pi} + 28 g_h^3\right)^2 - 48 c_1^{1/3} \left(15 j^2 \pi^2 + 32 \pi^{3/2} g_h^3\right)\right)}{6 c_1^{1/3} \sqrt{c_2}} \end{split}$$

Appendix C: Rotating Bardeen-AdS black holes with dark energy

$$\begin{split} P_{1S} &= 3180b^8\pi^4 - 6360b^4j^2\pi^4 - 3180b^6\pi^{7/2}\alpha + 6360b^6\pi^4\alpha - 9540b^6\pi^{7/2}\alpha\omega + 9540b^6\pi^4\alpha\omega, \\ P_{2S} &= -2610b^2j^2\pi^3S_c - 1305b^4\pi^{5/2}\alpha S_c + 3480b^4\pi^3\alpha S_c - 3915b^4\pi^{5/2}\alpha\omega S_c + 5220b^4\pi^3\alpha\omega S_c - 156b^4\pi^2S_c^2, \\ P_{3S} &= -540j^2\pi^2S_c^2 - 270b^2\pi^{3/2}\alpha S_c^2 + 876b^2\pi^2\alpha S_c^2 - 810b^2\pi^{3/2}\alpha\omega S_c^2 + 1314b^2\pi^2\alpha\omega S_c^2 - 83b^2\pi S_c^3, \\ P_{4S} &= +72\pi\alpha S_c^3 + 108\pi\alpha\omega S_c^3 + 6S_c^4), \\ \lambda_5 &= \left(12\lambda_3^{1/3}\left(358b^6\pi^3 + b^2\pi^{3/2}\left(870j^2\pi^{3/2} + \alpha\left(-15(1+3\omega) + 43\sqrt{\pi}(2+3\omega)\right)\left(9\pi\alpha(2+3\omega) - 2\sqrt{\lambda_4}\right) + b^4\pi^2\left(3\sqrt{\pi}\alpha\left(145(1+3\omega) - 358\sqrt{\pi}(2+3\omega)\right) + 55\sqrt{\lambda_4}\right) - 3\pi^2\left(9\pi\alpha(2+3\omega)\left(10j^2 + \alpha^2(2+3\omega)^2\right) - (20j^2 + 3\alpha^2(2+3\omega)^2)\sqrt{\lambda_4}\right) - 182^{1/3}\pi^3\left(17b^4\sqrt{\pi} - 30j^2\sqrt{\pi} + b^2\alpha(-15(1+3\omega) + 14\sqrt{\pi}(2+3\omega))\right)^2\sqrt{\lambda_4} - 2^{2/3}\lambda_3^{2/3}\sqrt{\lambda_4}\right) / \left(6\lambda_3^{1/3}\sqrt{\lambda_4}\right), \\ \lambda_4 &= \left(182^{1/3}\pi^3\left(17b^4\sqrt{\pi} - 30j^2\sqrt{\pi} + b^2\alpha\left(-15(1+3\omega) + 14\sqrt{\pi}(2+3\omega)\right)\right)^2 + 6\left(55b^4\pi^2 + 2b^2\pi^{3/2}\alpha\left(15 + 45\omega - 43\sqrt{\pi}(2+3\omega)\right) + 3\pi^2\left(20j^2 + 3\alpha^2(2+3\omega)^2\right)\right)\lambda_3^{1/3} + 2^{2/3}\lambda_3^{2/3}\right) / \left(6\lambda_3^{1/3}\right), \\ \lambda_3 &= 54\pi^{9/2}\lambda_1 + \sqrt{\lambda_2}, \\ \lambda_2 &= 2916\pi^9\left(-\left(17b^4\sqrt{\pi} - 30j^2\sqrt{\pi} + b^2\alpha\left(-15(1+3\omega) + 14\sqrt{\pi}(2+3\omega)\right)\right)^6 + \lambda_1^2\right), \\ \lambda_1 &= 4737b^{12}\pi^{3/2} - 27000j^6\pi^{3/2} + 2700b^2j^4\pi\alpha\left(-15(1+3\omega) + 14\sqrt{\pi}(2+3\omega)\right) + 3b^{10}\pi\alpha\left(-3155\right) \right) + 3b^{10}\pi\alpha\left(-3155\right) + 3b^{10$$

$$\begin{split} &(1+3\omega)+2574\sqrt{\pi}(2+3\omega))+b^{5}\alpha\left(-180j^{2}\pi\left(-355(1+3\omega)+414\sqrt{\pi}(2+3\omega)\right)+\alpha^{2}(-3375\left(1+3\omega)^{2}+9450\sqrt{\pi}(1+3\omega)^{2}(2+3\omega)-7920\pi(1+3\omega)(2+3\omega)^{2}+1576\pi^{3/2}(2+3\omega)^{3}\right)-3b^{5}\sqrt{\pi}\left(6310j^{2}\pi-\alpha^{2}\left(5325(1+3\omega)^{2}+7648\pi(2+3\omega)^{2}-12420\sqrt{\pi}\left(2+9\omega+9\omega^{2}\right)\right)\right),}\\ &(\pi(6310j^{2}\pi-\alpha^{2}(225(1+3\omega)^{2}+176\pi(2+3\omega)^{2}-4200\sqrt{\pi}\left(2+9\omega+9\omega^{2}\right)\right)),}\\ &P_{1L}=3180b^{3}n^{1+3\omega}\pi^{4}-6360b^{4}j^{2}n^{1+3\omega}\pi^{4}+6360b^{6}\pi^{4}\alpha+9540b^{6}\pi^{4}\alpha\omega-2610b^{2}j^{2}n^{1+3\omega}\pi^{3}S_{c},}\\ &P_{2L}=3480b^{4}\pi^{3}\alpha S_{c}+5220b^{4}\pi^{3}\alpha\omega S_{c}-156b^{4}n^{1+3\omega}\pi^{2}S_{c}^{2}-540j^{2}n^{1+3\omega}\pi^{2}S_{c}^{2}+876b^{2}\pi^{2}\alpha S_{c}^{2},}\\ &P_{3L}=1314b^{2}\pi^{2}\alpha\omega S_{c}^{2}-83b^{2}n^{1+3\omega}\pi S_{c}^{2}+72\pi\alpha S_{c}^{2}+108\pi\alpha\omega S_{c}^{2}+6n^{1+3\omega}S_{c}^{2},}\\ &\beta_{1}=4737b^{12}n^{3+6\omega}-27000j^{3}n^{3+6\omega}+7722b^{10}n^{2+6\omega}\alpha(2+3\omega)+37800b^{2}j^{4}n^{2+6\omega}\alpha(2+3\omega)-n^{1+3\omega}(6873155j^{2}n^{2+6\omega}-3824\alpha^{2}(2+3\omega)^{2})+180b^{4}j^{2}n^{1+3\omega}(355j^{2}n^{2+6\omega}-88\alpha^{2}(2+3\omega)^{2})+8b^{6}\alpha(2+3\omega)\\ &(-9315j^{2}n^{2+6\omega}+197\alpha^{2}(2+3\omega)^{2}),\\ &\beta_{2}=54\pi^{6}\beta_{1}+54\pi^{6}\sqrt{-(17b^{4}n^{1+3\omega}-30j^{2}n^{1+3\omega}+14b^{2}\alpha(2+3\omega))^{6}+\beta_{1}^{2},}\\ &\beta_{3}=n^{-2-6\omega}\left(18\cdot2^{1/3}n^{1+3\omega}\pi^{4}\left(17b^{4}n^{1+3\omega}-30j^{2}n^{1+3\omega}+14b^{2}\alpha(2+3\omega)\right)^{2}+6\pi^{2}\left(55b^{4}n^{2+6\omega}+n^{2+6\omega}+n^{2+6\omega}\right)\\ &\phi_{2}^{2}-86b^{2}n^{1+3\omega}\alpha(2+3\omega)+9\alpha^{2}(2+3\omega)^{2}\right)\beta_{2}^{2/3}+2^{2/3}n^{1+3\omega}\beta^{2/3}\right)/\left(6\beta_{2}^{1/3}\right),\\ &\beta_{4}=\left(12\pi^{2}\beta_{2}^{1/3}\left(358b^{6}n^{3+6\omega}\pi+b^{2}n^{1+3\omega}\left(870j^{2}n^{2+6\omega}\pi+43\alpha(2+3\omega)\left(9\pi\alpha(2+3\omega)-2n^{1+3\omega}+14b^{2}\alpha(2+3\omega)\right)+h^{1+3\omega}\left(20j^{2}n^{2+6\omega}+3\alpha^{2}(2+3\omega)^{2}\right)\beta_{3}\right)\right)-18\cdot2^{1/3}\eta^{2+6\omega}\pi^{4}\left(17b^{4}n^{1+3\omega}-30j^{2}n^{1+3\omega}+14b^{2}\alpha(2+3\omega)^{2}\right),\\ &\eta_{1}=\left(\frac{2\pi^{2}\beta_{2}^{1/3}}{358b^{6}n^{2+6\omega}}+3a^{2}(2+3\omega)^{2}\right)\beta_{3}\right)-18\cdot2^{1/3}\eta^{2+6\omega}\pi^{4}\left(17b^{4}n^{1+3\omega}-30j^{2}n^{1+3\omega}+14b^{2}\alpha(2+3\omega)^{2}\right),\\ &\eta_{1}=\left(\frac{2\pi^{2}\beta_{2}^{1/3}}{358b^{6}n^{2+6\omega}}+b^{2}n^{1+3\omega}\left(870j^{2}n^{2+6\omega}\pi+43\omega(2+3\omega)\left(9\pi\alpha(2+3\omega)-2n^{1+3\omega}+14b^{2}\alpha(2+3\omega)\right)\right),\\ &\eta_{1}=\left(\frac{2\pi^{2}\beta_{2}^{1/3}}{358b^{2}}+8pS^{\frac{3}2+\frac{3\omega}{2}}+3n^{3}\frac{3(1+\omega)}{35a^{2}}\alpha(2+3\omega)\right)\right),\\ &\eta_{2}=\left(\frac{2\pi^{2}\beta_{2}^{1/3}}{358b^{2}}+3n^{2}\beta_{2}^{2}$$